ISSN 1063-7842, Technical Physics, 2013, Vol. 58, No. 9, pp. 1329–1336. © Pleiades Publishing, Ltd., 2013.
Original Russian Text © I.A. Lyashenko, I.V. Vinnichenko, 2013, published in Zhurnal Tekhnicheskoi Fiziki, 2013, Vol. 83, No. 9, pp. 90–97.

PHYSICS OF NANOSTRUCTURES

Stick–Slip Melting of a Boundary Lubricant between Two Rigid Surfaces with Nanoscale Asperities

I. A. Lyashenko[a] and I. V. Vinnichenko[b]

[a] *Sumy State University, ul. Rimskogo-Korsakova 2, Sumy, 40007 Ukraine*
[b] *OOO NetCracker, Sumy, 40011 Ukraine*
e-mail: nabla04@ukr.net

Received September 27, 2012

Abstract—With a simple mechanical analog of the elastic tribological system, the friction of two rough surfaces is studied using the model of first-order phase transitions. The surfaces rub under boundary friction conditions in the presence of a lubricant layer in between. Stick–slip motion is considered, which is due to periodic phase transitions arising between kinetic friction conditions. It is shown that when rubbing surfaces are rough, a time-varying domain structure with a spatially distributed order parameter occurs in the plane of friction during motion.

DOI: 10.1134/S1063784213090193

INTRODUCTION

Boundary friction has been attracting the attention of researchers for more than a decade. More than a century ago, as early as in 1902, German scientist Richard Hermann Stribeck experimentally derived the dependence of the friction coefficient of a bearing on the rotation velocity in the presence of a lubricant. Subsequently, this dependence received the name of the Hersey–Stribeck diagram. In the case of a thin lubricant, the diagram shows the transition regime of boundary friction early in the motion of the bearing. According to the Hersey–Stribeck diagram, boundary friction is characterized by a high friction coefficient and, as a result, by elevated dissipation of mechanical energy. This leads to overheating of rubbing parts, which may eventually fail. Clearly, gaining a deeper insight into boundary friction conditions is of great applied significance. With the advent of advanced instrumentation, it became possible to directly observe complex processes occurring in the contact region [1, 2]. Recent experimental data [3–6] confirm and refine many intuitive inferences drawn both by domestic (Akhmatov, Epifanov, Deryagin, and others) and by foreign scientists (Hardy, Beer, Bowden) of the last century.

Under boundary friction conditions, the well-known Amontons' law often breaks. For example, in Hardy's experiments on friction between two plane surfaces with an aromatic compound layer in between, the static friction coefficient decreases with rising load [7]. Hardy explains this effect, assuming that low pressures effectively act as a multimolecular lubricant layer, which is nonfluid unlike thick lubricants. It thus can be supposed that there exist limiting internal stresses above which the lubricant becomes fluid. Hardy also concludes that a lubricant layer becomes thinner with increasing pressure, as a result of which the friction coefficient changes. In this way, Hardy introduced the dependence of the friction coefficient on the lubricant thickness. Exactly the same situation, when the lubricant thickness has a critical influence on friction conditions, is considered in this work. Hardy in his works notes that the lubricant can be named as neither a liquid nor solid. Today, researchers use the terms "liquidlike and solidlike states," which differ from equilibrium thermodynamic states, since the microrelief of rubbing surfaces considerably influences the lubricant, disturbing the symmetry of the state [8, 9].

Although investigation of the boundary friction conditions is of great scientific and fundamental significance, no unified theory of boundary friction has been developed to date. Because of the complexity of processes occurring in the contact region, phenomenological models are often used [8, 10–13]. In addition, related experimental data are successfully described by the methods of molecular dynamics [14–16]. Specifically, a synergetic model was suggested [17, 18] in which a lubricant layer is assumed to melt following the mechanisms of dynamic and shear-induced melting. Popov [8, 10] developed a thermodynamic theory of boundary friction based on the Landau theory of second-order transitions [19]. In the latter, the shear modulus of the lubricant, which vanishes in the liquidlike phase, is taken for the order parameter. However, under the boundary friction conditions, stepwise first-order phase transitions, which cause the stick–slip friction mode to set in, typically occur [9, 12, 20]. In this connection, Lyashenko [22, 23] generalized the Popov theory [8, 10] for the case when the

first-order phase transition takes place. In [22, 23], the specific situation of atomically smooth surfaces is analyzed. However, this situation is sometimes encountered in practice and is extensively studied experimentally [5, 6, 9, 20]. This work, pursuing works [22, 23], is aimed at theoretically studying the boundary friction conditions when rubbing surfaces have nanoscale asperities. Since in practice friction surfaces are almost always rough and inhomogeneous, such a consideration will help to extend previous data and cover a wider class of real tribological systems.

1. FREE ENERGY AND PHASE DIAGRAM

In the homogeneous case, the expression for the free energy density of a lubricant layer in between two solid surfaces can be represented in the form [8, 10, 22, 23]

$$f = \alpha(T - T_c)\varphi^2 + \frac{a}{2}\varphi^2\varepsilon_{el}^2 - \frac{b}{3}\varphi^3 + \frac{c}{4}\varphi^4, \quad (1)$$

where T is the lubricant temperature; T_c is the critical temperature; ε_{el} is the shear component of elastic strain; and α, a, b, and c are positive constants. Order parameter φ is the amplitude of the periodic part of the microscopic density function of the medium [8, 10]. Thus, the liquidlike phase of the lubricant has a constant value of φ, $\varphi_0 = 0$, whereas in the solidlike phase, $\varphi_0 > 0$. Here (unlike in [8, 10]), expansion (1) corresponds to the model of the first-order phase transition developed in [19, 22–24].

Since parameter φ is the density modulation, hereinafter the range $\varphi \geq 0$ will be considered. In expression (1), one can distinguish critical melting point T_{c0} and critical solidification point T_c^0 of the lubricant, T_{c0} exceeding T_c^0 ($T_{c0} > T_c^0$) by a constant value depending on only expansion constants [22, 23],

$$T_{c0} = T_c - \frac{a}{2\alpha}\varepsilon_{el}^2 + \frac{b^2}{8\alpha c}, \quad (2)$$

$$T_c^0 = T_c - \frac{a}{2\alpha}\varepsilon_{el}^2. \quad (3)$$

In the temperature range $T_c^0 < T < T_{c0}$, the curve $\varphi_0(T, \varepsilon_{el})$ exhibits a hysteresis, which is characteristic of first-order phase transitions [22, 23]. Note that during melting order parameter φ changes stepwise from constant value $\varphi_0 = 0.5b/c$ to zero, whereas during solidification, φ grows from zero to $\varphi_0 = b/c$ [22, 23].

When surfaces are rubbing in the presence of a lubricating layer, the lubricant experiences elastic stresses σ_{el}, which are defined as the derivative of free energy f given by (1) with respect to strain ε_{el},

$$\sigma_{el} = \mu\varepsilon_{el}, \quad (4)$$

where shear modulus μ equals the order parameter squared up to constant factor a [8, 10, 22, 23],

$$\mu = a\varphi^2. \quad (5)$$

The friction force, which offers resistance to the motion of the surfaces, is given by the formula [12, 22, 23, 25]

$$F = \left[\sigma_{el} + k\,\mathrm{sgn}(V)\left(\frac{|V|}{h}\right)^{\gamma+1}\right]A, \quad (6)$$

where A is the contact area between rubbing surfaces, h is the lubricant thickness, and k and γ are phenomenological parameters specifying the type of lubricant [21, 26]. In particular, $\gamma < 0$ refers to the non-Newtonian pseudoplastic lubricant. The second term in (6) describes viscous stresses, which exist only when the surfaces move with relative velocity $V \neq 0$. The friction force appearing in formula (6) is proportional to the contact surface area A and does not depend on the load on the surface. This is because we are considering the specific conditions of friction between two surfaces with nanoscale asperities that are separated by a simple nonpolar lubricant, the distance between them being kept constant in motion. In this case, the surface area of a real contact (contact through lubricant) is close to the areas of the rubbing surfaces irrespective of the applied pressure and formula (6) is applicable. Then, the notion of the friction coefficient becomes meaningless [27].

It was shown [12, 22, 23, 28] that when rubbing surfaces move with relative velocity V, stationary elastic strain arises in the lubricant layer,

$$\varepsilon_{el}^0 = \frac{V\tau_\varepsilon}{h}, \quad (7)$$

where τ_ε is the Maxwell time of internal stress relaxation [8]. At $\tau_\varepsilon \ll 1$, expression (7) can be used to determine strain ε_{el} with a good accuracy. Using expressions (2) and (3) for the temperatures with regard to (7), one can derive similar expressions for the critical velocities [22, 23],

$$V_{c0} = \frac{h}{\tau_\varepsilon}\sqrt{\frac{2\alpha(T_c - T)}{a} + \frac{b^2}{4ac}}, \quad (8)$$

$$V_c^0 = \frac{h}{\tau_\varepsilon}\sqrt{\frac{2\alpha(T_c - T)}{a}}. \quad (9)$$

Figure 1 shows the phase diagram of the lubricant. It represents the temperature dependences of velocities V_{c0} and V_c^0. Above the curve for V_{c0}, the lubricant is liquidlike (potential $f(\varphi)$ has a single minimum at $\varphi = 0$) and the sliding friction (SF) conditions set in. At $V < V_c^0$, the lubricant has a solidlike structure (the potential has a single minimum at $\varphi > 0$) and friction is dry (DF). In between the curves, potential $f(\varphi)$ at positive φ has both zero and nonzero minima with a maximum between them. Thus, the state of the material depends on initial conditions in this intermediate interval. Figure 1 can be considered as the depen-

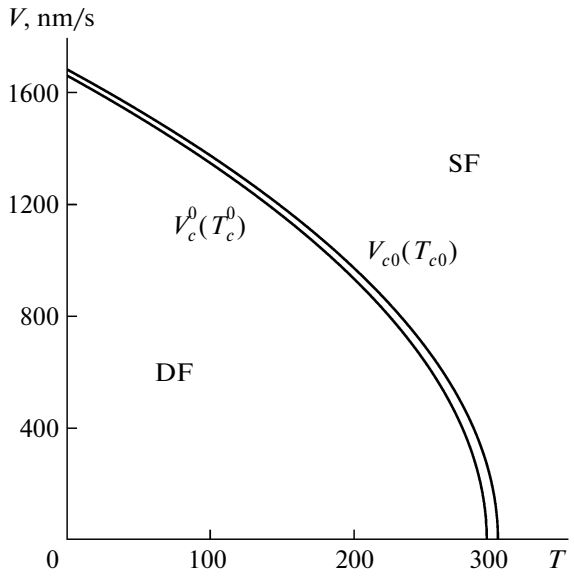

Fig. 1. Phase diagram with liquidlike (sliding friction) and solidlike (dry friction) states of a lubricant at $\alpha = 0.95$ J K^{-1}/m^3, $T_c = 290$ K, $a = 2 \times 10^{12}$ Pa, $b = 230$ J/m^3, $c = 900$ J/m^3, $h = 10^{-9}$ m, and $\tau_\varepsilon = 10^{-8}$ s.

dences of critical temperatures T_{c0} given by (2) and T_c^0 given by (3) on shear rate V.

2. LUBRICANT MELTING KINETICS

The typical tribological system [8, 9, 20] the behavior of which was studied in terms of the adopted model earlier [23] is depicted in Fig. 2. Note that in our previous works rubbing surfaces were assumed to be atomically smooth, whereas here we study boundary friction between rough surfaces. The system shown in Fig. 2 consists of a spring with stiffness K and mass M, which slides over a surface covered by an h-thick lubricant. Thickness h is a variable parameter, varying from point to point in motion. The free end of the spring is put in motion with fixed velocity V_0. When the mass slides over the surface, friction force F, which is determined from formula (6), arises between them.

Let us write the equation of motion of the mass with coordinate X in the form [8, 9, 23]

$$M\ddot{X} = K(V_0 t - X) - F, \tag{10}$$

where the parenthesized expression is extension ΔX of the spring and t is the time of motion of its free end. Equation (10) should be complemented by the Landau–Khalatnikov kinetic equation [23, 29],

$$\dot{\varphi} = -\delta\frac{\partial f}{\partial \varphi}, \tag{11}$$

which in the explicit form appears as

$$\dot{\varphi} = -\delta(2\alpha(T - T_c)\varphi + a\varphi\varepsilon_{el}^2 - b\varphi^2 + c\varphi^3) + \xi(t). \tag{12}$$

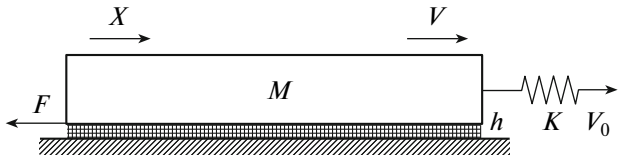

Fig. 2. Tribological system.

Here, δ is the kinetic coefficient and $\xi(t)$ is an additional stochastic term standing for small additive fluctuations. These fluctuations should be taken into account because of the specific features of subsequent numerical calculation [22, 23]. In the simplest case, process $\xi(t)$ is represented as white noise with moments

$$\langle \xi(t) \rangle = 0; \quad \langle \xi(t)\xi(t') \rangle = 2D\delta(t - t'), \tag{13}$$

where intensity D of a stochastic source is everywhere set equal to 10^{-25} s^{-1}.

Figure 3 shows the friction surface relief generated with the well-known hill algorithm. This algorithm uses iterations, and its essence is the following. First, a 2D $N \times N$ array is created and filled with zero values. The value of an element in the array is height z of a given point on the surface, and the indices of an element are the integer-valued coordinates of point (x, y). Thus, we initially have a plane. Then, coordinates (x_r, y_r) are randomly selected; moreover, they can be selected outside the array (surface) as well. At this step, one more random quantity, radius r of a hill, is generated. Range r of random quantities considerably influences the final relief of the surface. Then, heights z are calculated for all elements (i.e., points (x, y) on the surface) of the array by the formula

$$z = r^2 - (x - x_r)^2 - (y - y_r)^2. \tag{14}$$

If $z(x, y) > 0$, height z is added to the value of the respective element, random point (x_r, y_r) and random radius r are generated again, and the above procedure is repeated. Let it be repeated n times. Note that parameter n considerably influences the relief of the surface obtained with the hill algorithm. After the procedure is complete, heights z of the surface are scaled from 0 to 1 and the resulting surface is lowered down to a zero level. This can be easily done by calculating all heights $z(x, y)$ according to the relationship

$$z := \frac{z - z_{\min}}{z_{\max} - z_{\min}}, \tag{15}$$

where $z_{\min}$ and $z_{\max}$ are the minimal and maximal values of z in the array before scaling. Surfaces depicted in Fig. 3 were obtained in this way. The upper surface (on the left) in the plane xy has 200×200 points; the lower (on the right), 400×200. Random radius r was selected from the interval 0–50 for both surfaces. The number of iterations for the upper surface was $n = 1000$; for the lower surface, $n = 2000$ (the surface area of the latter is twice as large). Coordinates x_r and y_r

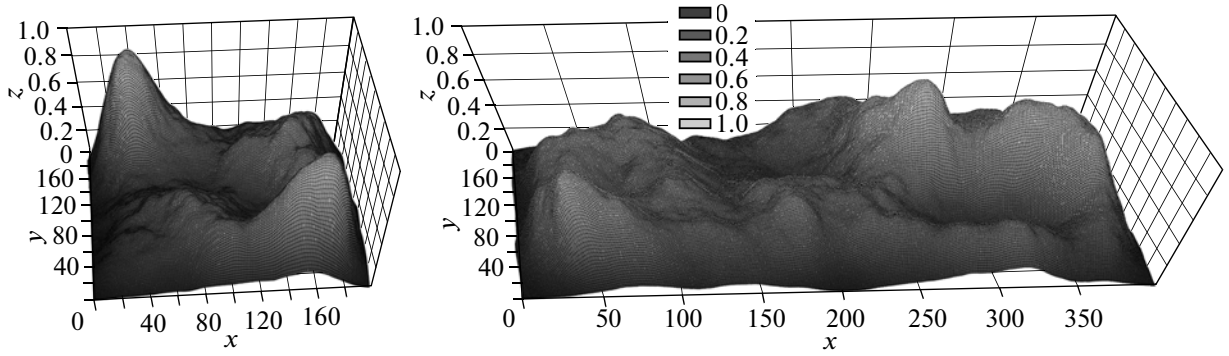

Fig. 3. General view of the upper (on the left) and lower (on the right) rubbing surfaces obtained by using the hill algorithm.

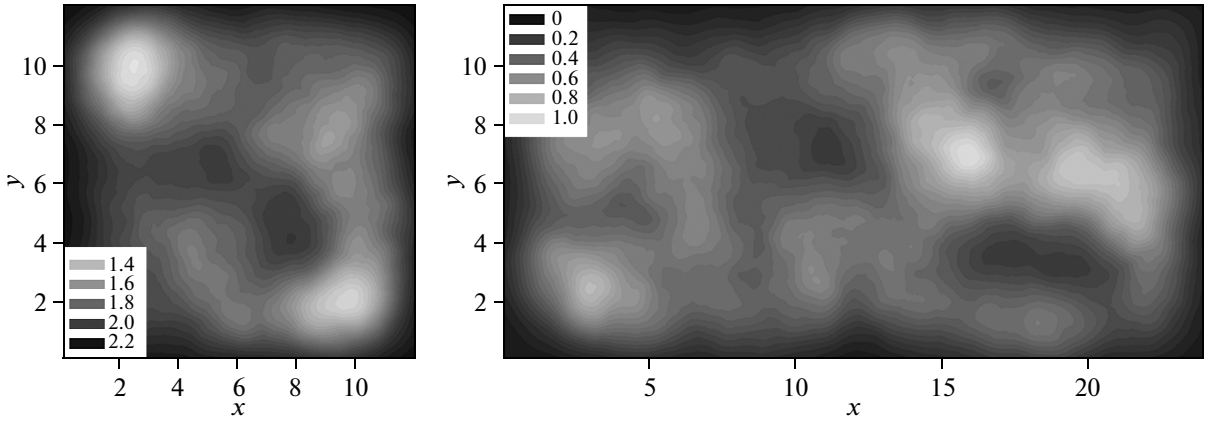

Fig. 4. Height maps for the upper (on the left) and lower (on the right) rubbing surfaces after scaling. Coordinates x and y are given in micrometers; heights on the legends, in nanometers.

used to generate both surfaces were selected in the range of the array; that is, both coordinates were taken from the interval 0–199 for the upper surface and from the intervals $y = 0$–199 and $x = 0$–399 for the lower one. After the surfaces were thus constructed, each value of z was squared to "lower" the edges of the surfaces and "raise" asperities relative to the normal pattern.

Once the surfaces are generated, they should be matched to the problem being considered. Since the upper surface will slide over the lower one, all points of the former should be inverted about the plane xy; that is, all elements of the array should be rearranged according to the relationship $z := 1 - z$. Then, crossing between the surfaces should be avoided (the asperity heights on the upper and lower surfaces fall into the range 0–1). To this end, for each fixed coordinate y, the minimal value of the height, $z_{\min}$, is found on the upper surface; the maximal value of the height, $z_{\max}$, is found on the lower surface; and the difference $\Delta z = z_{\min} - z_{\max}$ is determined. In this way, we obtain 200 values of Δz for all available axes y. The minimal value of these differences, $\Delta z_{\min}$, is selected, and the upper surface is brought into contact with the lower one along the path according to the relationship $z := z - \Delta z_{\min}$. Under these conditions, the surfaces will not overlap when moving but will touch each other at some points (at least at one). Next, each element of both arrays on the surfaces is multiplied by $l = 10^{-9}$ m, as a result of which the upper surface rises by 0.5 nm according to the substitution $z := z + 0.5 \times 10^{-9}$ m. Let the linear size of the upper square surface be $L = 1.2 \times 10^{-5}$ m. In this case, the area of this surface is $A = L^2 = 0.144 \times 10^{-9}$ m^2 and the distance between points along the x and y axes is

$$S_{x,y} = \frac{L}{200} = 6 \times 10^{-8} \text{ m}. \quad (16)$$

Eventually, we have two surfaces with necessary sizes, nanoscale asperities, and identical properties.

Figure 4 shows the scaled surfaces in the form of height maps in which coordinates x and y stand not for the number of points (as in Fig. 3) but for spatial coordinates (in micrometers) and the lower left-hand angle is taken for the point of reference. Shades of gray in the legend to Fig. 3 indicate the values of heights on the surfaces in nanometers. Since the upper surface was inverted in preparation, its asperities now correspond

to smaller values of z. Therefore, for bright areas in Fig. 4 to correspond to asperities on both surfaces, the heights increase from brighter areas to darker ones on the left-hand surface and from darker areas to brighter ones on the right-hand surface.

Let us consider the kinetics of the system depicted in Fig. 2 when the surfaces shown in Fig. 4 act as upper and lower rubbing surfaces. First, it is necessary to numerically solve differential equations (10) and (12) with regard to definitions (4)–(7) and (13). Since the contact area contains $200 \times 200 = 40\,000$ domains, quantities $h[i][j]$, $\varepsilon_{el}[i][j]$, $\varphi[i][j]$, $\sigma_{el}[i][j]$, and $F[i][j]$ are determined at each step of numerical integration for each domain separately. Here, i is the integer-valued index of a point on the surface along the X axis and j is the index corresponding to the Y axis (both indices vary from 0 to 199). It is assumed that the lubricant temperature T is constant for all domains; that is, we consider an ultrathin lubricant, in which case excess heat arising at motion in the contact zone, is rapidly transferred to a friction surface (thermostat or environment). It should be noted that, when the upper surface moves, quantities $h[i][j]$ vary, because these heights are the distances between the respective points on the upper and lower rubbing surfaces. This fact is taken into account by introducing the integer-valued variable

$$s = \text{integer}\left(\frac{X}{S_{x,y}}\right), \qquad (17)$$

which describes the shift of the upper surface relative to the lower one. Here, X is the coordinate of the upper rubbing surface, which equals zero at the zero time ($t = 0$), and $S_{x,y}$ (see (16)) is the distance between surface points along the X axis. Then, $h[i][j]$ can easily be determined as

$$h[i][j] = \text{top}[i][j] - \text{bottom}[i+s][j], \qquad (18)$$

where top[200][200] is the array of scaled heights on the upper surface and bottom[400][200] is the array of heights on the lower surface. From expression (18) it follows that the upper surface shifts toward the X axis, because coordinates Y (index j) on both surfaces remain unchanged during motion. When solving equation of motion (10), we will numerically solve differential equation (12) at each time step separately for each domain to find the current values of order parameter $\varphi[i][j]$, which depend on the previous values of array $\varphi[i][j]$. Initially ($t = 0$), all elements from array $\varphi[i][j]$ are assigned value $\varphi_0 = 0.5$; that is, the lubricant is assumed to be homogeneous in composition and be in the solidlike state. Then, knowing the order parameters for all domains, their contribution to the friction force is calculated by modified formula (6),

$$F[i][j] = \left[\sigma_{el}[i][j] + k\,\text{sgn}(V)\left(\frac{|V|}{h[i][j]}\right)^{\gamma+1}\right]\frac{L^2}{N^2}, \qquad (19)$$

where $A = L^2 = 0.144 \times 10^{-9}$ m^2 is the surface area of the contact introduced above and N^2 is the total number of domains. After quantities (19) are calculated, the effective friction force is found as a sum of all elements of the array (a total of $N^2 = 40\,000$ elements) and this value is used to solve kinetic equation (10). Solving Eq. (10), one finds new values of X, V, and ΔX; then, the procedure is repeated. In (19) velocity V is not indexed, since the upper surface is perfectly rigid and moves as a whole.

The above equations were numerically integrated using the Euler iteration method [22, 23] with time step $\Delta t = 10^{-7}$ s. The iteration procedure lasts until integer-valued shift variable s given by (17) becomes equal to 200, that is, until the upper surface reaches the end of the lower one. For the above values of the parameters, this requires more than 9×10^7 iterations and $N^2 = 40\,000$ values of arrays $h[i][j]$, $\varepsilon_{el}[i][j]$, $\varphi[i][j]$, $\sigma_{el}[i][j]$, and eventually $F[i][j]$ must be calculated at each iteration. This considerably slows down numerical calculation, making it unrealistic for present-day PCs. However, since domains do not interact with each other in the approach adopted, the values of the arrays are also calculated independently at each step. Therefore, we can apply the Compute Unified Device Architecture (CUDA) parallel computing architecture developed by NVIDIA in 2007 [30]. This architecture is used for nongraphic computation with general-purpose graphic processors of NVIDIA video adapters. Since equation of motion (10) is calculated on a central processor unit after total friction force F has been numerically determined as a sum of partial friction forces (see (19)), the frequency of the central processor unit considerably influences the time of numerical calculation as well. We used an Intel Core 2 Quad Q9400 central processor unit with a clock frequency of 2.66 GHz and a Palit GeForce GTX 570 Sonic 1280 MB video adapter having 480 general-purpose processors with a clock frequency of 1.4 GHz. The program execution time (the time taken to calculate the dependences in Fig. 5) was 5 h 32 min.

The dependences obtained by solving the above equations are shown in Fig. 5. At a given temperature, the lubricant at rest ($\varepsilon_{el} = 0$) is solidlike. At the zero time ($t = 0$), the free end of the spring starts uniformly moving with velocity $V_0 = 1.4$ μm/s. Initially, variable s standing for shift is zero as a result of which the components of friction force (19) grow with velocity V in all domains. As the velocity grows, so do elastic strains $\varepsilon_{el}[i][j]$, which, in turn, increases elastic stresses $\sigma_{el}[i][j]$. Since initially velocity V is much lower than V_0, the spring elongates and extension ΔX grows. With time, coordinate X increases, variable s (17) becomes other than zero, and $h[i][j]$ is recalculated. This all disturbs the periodicity of the dependences, which is particularly noticeable in the dependence $V(t)$. For each domain, the melting condition $V > V_{c0}$ will be fulfilled at different instants of time, because critical velocity V_{c0} (8) is proportional to the distance between the "planes" of surfaces $h[i][j]$ bounding the respective

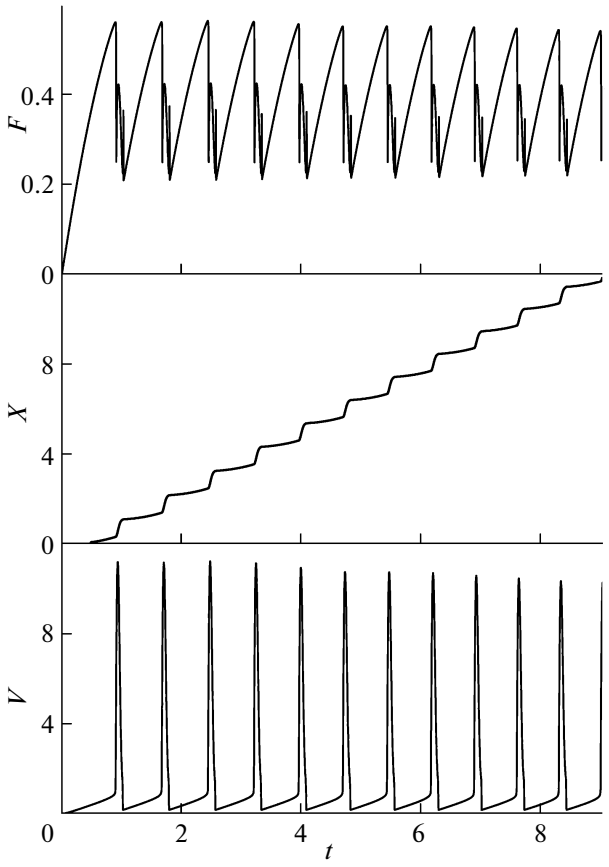

Fig. 5. Friction force F (mN), coordinate X of the upper mass (μm), and velocity V (μm/s) of the upper mass vs. time t (s) for the same parameters as in Fig. 1 and $k = 1.5 \times 10^5$ Pa s$^{1/3}$, $\gamma = -2/3$, $\delta = 100$ J^{-1} m^3/s, $K = 600$ N/m, $M = 0.5$ kg, $T = 200$ K, and $V_0 = 1400$ nm/s.

domains. Therefore, at each instant of time, the lubricant is solidlike at one site of the surface and liquidlike at others. However, at some instants, motion velocity V rises manifold, as follows from Fig. 5. Such a situation corresponds to complete melting of the lubricant, since, when velocity V sharply grows, the condition $V > V_{c0}$ is met in all domains. At melting, stresses $\sigma_{el}[i][j]$ vanish and slip velocity V of the upper mass rises, because elastic components $F[i][j]$ of the friction force also vanish. In this situation, the mass rapidly travels a large distance, as indicated by the increased slope of the dependence $X(t)$ after melting. Since now the mass moves with velocity V far exceeding velocity V_0 of the free end of the spring, the spring shrinks and extension ΔX, together with elastic force $K\Delta X$ causing motion, decreases. Again, the condition $V < V_c^0$ in the domains is met at different instants of time; therefore, an inhomogeneous domain structure forms at solidification. It should be noted that the dependences depicted in Fig. 5 have a nearly periodic form but are not strictly periodic, as also follows from investigations into the behavior of rough surfaces interacting in motion with regard to elasticity [31]. Note that the stick–slip motion shown in Fig. 5 was described by Bowden and Tabor as early as 50 years ago [32] in experiments on the influence of the molecular height of polymers on the friction coefficient.

Consider in greater detail switchover between the kinetic conditions of sliding friction and dry friction. Figure 6 plots the same time dependences of friction force F and slip velocity V but within a limited time interval. In this figure, the distribution of order parameter φ over the sliding surface at four instants of time is shown. Coordinates x and y in Fig. 6 correspond to the values shown in Fig. 4 for the upper rubbing surface. Coordinates X of points on the upper rubbing surface can be calculated as

$$X = x + sS_{x,y}, \tag{20}$$

where shift variable s (17) takes values of 161, 162, 174, and 174 for the four increasing time instants in Fig. 6. Let us analyze these data. It is seen from the dependence $F(t)$ that at $t = 7.57$ s the dry friction conditions set in the system. In this case, the friction force is high and motion velocity V is low. It is seen in the respective spatial distribution $\varphi(x, y)$ that the order parameter is almost everywhere positive ($\varphi > 0$); however, there are dark areas, where the lubricant is close to the liquidlike state. Since the number of domains with a solidlike lubricant many times exceeds the number of domains with a liquidlike structure, the dry friction conditions set in. At the instant $t = 7.61$ s, the sliding friction arises, since the friction force drastically drops and the sliding velocity grows. From the respective dependence $\varphi(x, y)$ it follows that $\varphi \sim 10^{-14}$ throughout the contact area, which meets selected intensity D (see (13)) of white noise. Thus, all domains are in the molten state. At the next instant of time $t = 7.73$ s, friction force F grows and sliding velocity V drops (a kink is observed in the dependence $V(t)$ at this instant of time when F increases). That is, the dry friction conditions are established in the system. However, some domains are still in the liquidlike state, as follows from the respective curve $\varphi(x, y)$. Moreover, the number of domains with the liquidlike structure (dark areas in the dependence) even exceeds the number of solidlike domains at this time instant. After complete solidification ($t = 7.74$ s), $\varphi > 0$ in all domains but darker areas, in which the shear modulus is lower, are observed in the respective dependence $\varphi(x, y)$. Note that dependences $\varphi(x, y)$ for the last two instants of time are characterized by the same values of s, $s = 174$. This suggests that the radical difference between these instants of time is in relaxation processes in the lubricant, rather than in sets of values of $h[i][j]$. If parameter s during motions remains constant for a long time, the curve $\varphi(x, y)$ is fully controlled by the set of $h[i][j]$ with other parameters fixed. This is because for given kinetic coefficient δ, order parameter φ rapidly relaxes to a stable value determined by quantity h. However, the relaxation time in tribological systems with nanometer

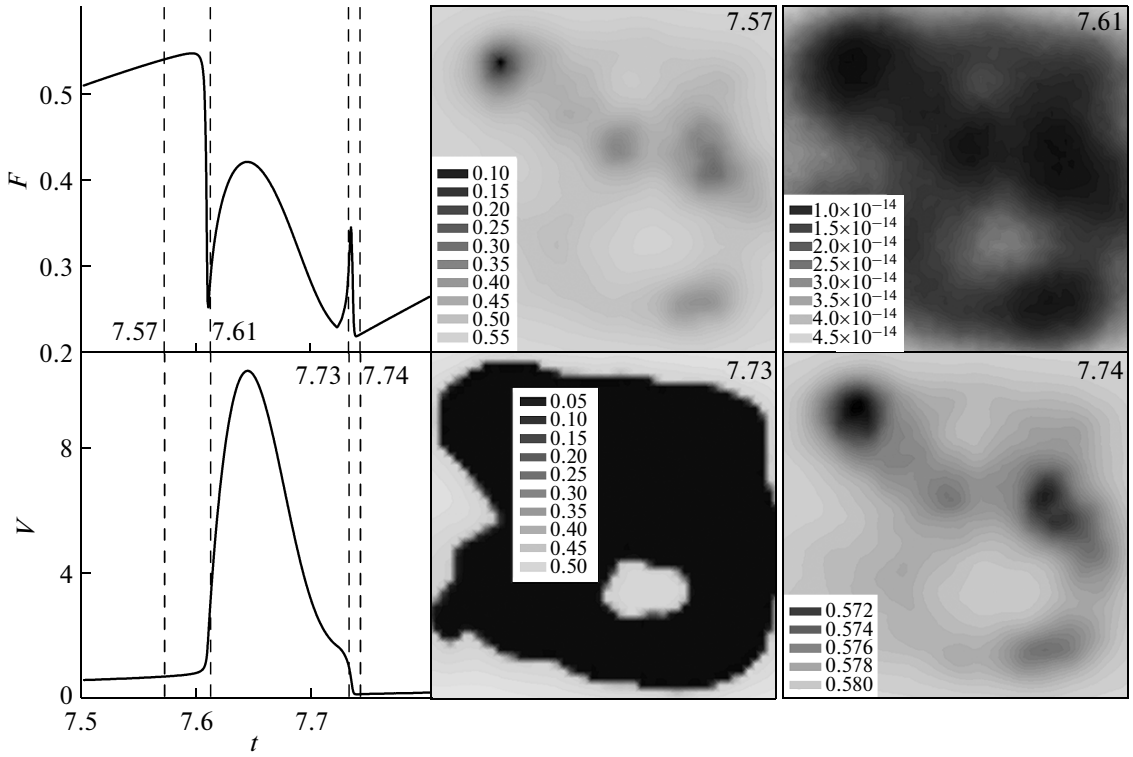

Fig. 6. Dependences $F(t)$ and $V(t)$ (see Fig. 5) within the time interval $t \in [7.5, 7.8]$ (s) and the distribution of order parameter $\varphi(x, y)$ over the contact surface at time instants of 7.57, 7.61, 7.73, and 7.74 s.

lubricants may differ by several orders of magnitude (depending on conditions) from that in systems with thick lubricants. Therefore, if necessary, one can adequately treat observations, such as the memory effects (when the relaxation time many times exceeds the observation time in experiments) by varying the value of δ [9]. Note that the features of the time dependence of the friction force shown in Fig. 6 (two post-melting peaks) were described in detail elsewhere [23].

CONCLUSIONS

In this work, a theoretical model of boundary friction based on the Landau theory of phase transitions is considered. The model makes it possible to represent the stick–slip friction as periodically occurring first-order phase transitions between the structural states of an ultrathin lubricant film in between two solid surfaces with nanoscale asperities. It is found that during friction between rough surfaces, the lubricant distributed over the area of the contact has a domain structure with liquidlike and solidlike portions variously contributing to the total friction force. It is shown that the time variation of the friction force for rough surfaces is not strictly periodic but has a nearly periodic form in agreement with experimental data. Calculations were carried out with the CUDA parallel computing architecture, which was developed by NVIDIA. This architecture is now widely used for nongraphic computation using a large number of general-purpose graphic processors in advanced video adapters. Earlier, we analyzed the behavior of indefinitely large atomically smooth surfaces with uniformly distributed lubricant properties. The results of this work obtained using this relatively new technology extend data for atomically smooth surfaces.

ACKNOWLEDGMENTS

This work was supported by the Ministry of Education and Science of Ukraine in the framework of project no. 0112U001380 “Simulation of Friction between Metallic Nanoparticles and Boundary Films of Liquids Interacting with Atomically Smooth Surfaces” and by a grant of the Cabinet of Ministers of Ukraine.

REFERENCES

1. B. N. J. Persson, *Sliding Friction: Physical Principles and Applications* (Springer, New York, 2000).
2. J. Israelachvili, Surf. Sci. Rep. **14**, 109 (1992).
3. S. Ohnishi, D. Kaneko, J. P. Gong, Y. Osada, A. M. Stewart, and V. V. Yaminsky, Langmuir **23**, 7032 (2007).
4. S. Yamada, Langmuir **24**, 1469 (2008).
5. A. L. Demirel and S. Granick, J. Chem. Phys. **109**, 6889 (1998).

6. G. Reiter, A. L. Demirel, J. Peanasky, L. L. Cai, and S. Granick, J. Chem. Phys. **101**, 2606 (1994).
7. W. Hardy and J. Bircumshaw, Proc. R. Soc. Lond. A **108**, 1 (1925).
8. V. L. Popov, Tech. Phys. **46**, 605 (2001).
9. H. Yoshizawa and J. Israelachvili, J. Phys. Chem. **97**, 11300 (1993).
10. V. L. Popov, Solid State Commun. **115**, 369 (2000).
11. A. E. Filippov, J. Klafter, and M. Urbakh, Phys. Rev. Lett. **92**, 135503 (2004).
12. I. A. Lyashenko, A. V. Khomenko, and L. S. Metlov, Tech. Phys. **55**, 1193 (2010).
13. I. A. Lyashenko, A. V. Khomenko, and L. S. Metlov, J. Friction Wear **32**, 113 (2011).
14. O. M. Braun and A. G. Naumovets, Surf. Sci. Rep. **60**, 79 (2006).
15. I. M. Sivebaek, V. N. Samoilov, and B. N. J. Persson, Langmuir **26**, 8721 (2010).
16. M. O. Robbins and M. H. Müser," Computer simulations of friction, lubrication and wear," *Modern Tribology Handbook*, Ed. by B. Bhushan (CRC, Boca Raton, 2001), pp. 717–765; cond-mat/0001056.
17. A. V. Khomenko and I. A. Lyashenko, J. Phys. Studies **11**, 268 (2007).
18. A. V. Khomenko, I. A. Lyashenko, and V. N. Borisyuk, Ukr. J. Phys. **54**, 1139 (2009).
19. L. D. Landau and E. M. Lifshitz, *Course of Theoretical Physics*, Vol. 5: *Statistical Physics* (Pergamon, Oxford, 1980), Part 1.
20. A. D. Berman, W. A. Ducker, and J. N. Israelachvili, Langmuir **12**, 4559 (1996).
21. G. Luengo, J. Israelachvili, and S. Granick, Wear **200**, 328 (1996).
22. I. A. Lyashenko, Tech. Phys. **56**, 869 (2011).
23. I. A. Lyashenko, Tech. Phys. **57**, 17 (2012).
24. V. L. Popov, Tech. Phys. Lett. **25**, 815 (1999).
25. I. A. Lyashenko, A. V. Khomenko, and L. S. Metlov, Tribol. Int. **44**, 476 (2011).
26. I. M. Sivebaek, V. N. Samoilov, and B. N. J. Persson, Phys. Rev. Lett. **108**, 036102 (2012).
27. A. S. Akhmatov, *Molecular Physics of Boundary Friction* (Israel Program for Scientific Translations, Jerusalem, 1966).
28. I. A. Lyashenko, Tech. Phys. **56**, 701 (2011).
29. L. D. Landau and I. M. Khalatnikov, Dokl. Akad. Nauk SSSR **96**, 469 (1954).
30. D. Sanders and E. Kandrot, *CUDA by Examples: An Introduction to General-Purpose GPU Programming* (Addison-Wesley, 2010).
31. U. Tartaglino, V. N. Samoilov, and B. N. J. Persson, J. Phys.: Condens. Matter. **18**, 4143 (2006).
32. F. P. Bowden and D. Tabor, *The Friction and Lubrication of Solids* (Clarendon, Oxford, 1954).

Translated by V. Isaakyan